Smart Structures and Systems, *Vol. 30, No. 6 (2022) 627-637*
https://doi.org/10.12989/sss.2022.30.6.627

The influences of equivalent viscous damping ratio determination on direct displacement-based design of un-bonded post-tensioned (UPT) concrete wall systems

Anqi Gu [1a] and Shao-Dong Shen*[2]

[1] *Department of Mechanical Engineering, University of Canterbury, Christchurch, New Zealand*
[2] *Disaster Prevention Research Institute, Kyoto University, Uji 611-0011, Japan*

(*Received May 12, 2022, Revised September 13, 2022, Accepted September 25, 2022*)

Abstract. Recent years, direct displacement-based design (DDBD) procedure is proposed for the design of un-bonded post-tensioned (UPT) concrete wall systems. In the DDBD procedure, the determination of the equivalent viscous damping (EVD) ratio is critical since it would influence the strength demand of the UPT wall systems. Nevertheless, the influence of EVD ratio determination of the UPT wall systems were not thoroughly evaluated. This study was aimed to investigate the influence of different EVD ratio determinations on the DDBD procedure of UPT wall systems. Case study structures with four, twelve and twenty storeys have been designed with DDBD procedure considering different EVD ratio determinations. Nonlinear time history analysis was performed to validate the design results of those UPT wall systems. And the simulation results showed that the global responses of the case study structures were influenced by the EVD ratio determination.

Keywords: direct displacement-based design; equivalent viscous damping ratio determination; nonlinear time histories analysis; un-bonded post-tensioned concrete wall

1. Introduction

In the 1990s, un-bonded post-tensioned (UPT) wall system is proposed as a precast concrete structural system to resist seismic action while suffering minimal damage (Kumara *et al*. 1999). Many cyclic loading tests (Erkmen and Schultz 2009, Gu *et al*. 2019, Holden *et al*. 2003, Perez *et al*. 2007, Restrepo and Rahman 2007, Van der Meer *et al*. 2013) of the UPT wall system evidenced that the seismic response of the UPT wall system is desirable. Compared with conventional precast concrete wall structures, the UPT wall structure has quick function recovery ability after earthquake action because of the rocking mechanism at the wall base (Nagae *et al*. 2014). As plotted in Fig. 1, the UPT wall consists of UPT tendons, precast concrete panels and energy dissipating devices. The UPT bars can provide restoring forces at the wall base after the wall panels start rocking. Energy dissipating devices, including internal reinforcing bars (Smith *et al*. 2011) and external steel fuses (Liu *et al*. 2018, Bedriñana *et al*. 2021), are arranged at the wall base to enhance the energy dissipation ability of the UPT walls. Previous results of cyclic loading tests showed that the hysteresis response of UPT wall system is characterized as a flag-shaped response (Erkmen and Schultz 2009, Gu *et al*. 2019, Holden *et al*. 2003, Restrepo and Rahman 2007).

Performance-based design of a structure is developed in recent years since it enables engineers to design structures performance based on its ultimate limit state, and performance-based warning methods are also developed to monitor the structure response in its lifetime (Huang *et al*. 2020, Zheng *et al*. 2021). The direct displacement-based design (DDBD) procedure proposed by Priestley (Priestley 2002) is one of the performance-based design methods by first determining the structures displacement profile at the design limit state. And a multi-degree-of-freedom (MDOF) structural system could be equivalent to a single-degree-of-freedom (SDOF) system by the design displacement profile and the equivalent viscous damping (EVD) ratio. The strength demand of the structural system is then obtained by the target displacement of the equivalent SDOF system and the reduced design displacement spectrum considering the EVD ratio. When applying the DDBD procedure to the UPT wall system, displacement profile and EVD ratio of that structural system should be first determined. The displacement profile of the UPT wall systems at design limit state was proposed for the DDBD procedure (Pennucci *et al*. 2009). Rahman and Sritharan (2006) have compared the DDBD procedure and force-based design (FBD) procedure for the UPT wall systems, and this study showed that the strength demand of DDBD procedures were reduced compared with that of FBD procedures, so the DDBD procedure was a more economical design procedure for the UPT wall system than the FBD procedure. Previous researches have stated the EVD ratio is a critical parameter in the DDBD procedure, and different EVD ratio

*Corresponding author,
JSPS International Research Fellow,
E-mail: ssd15@tsinghua.org.cn
[a] Post Doctoral Fellow, E-mail: anqi.gu@canterbury.ac.nz

ISSN: 1738-1584 (Print), 1738-1991 (Online)

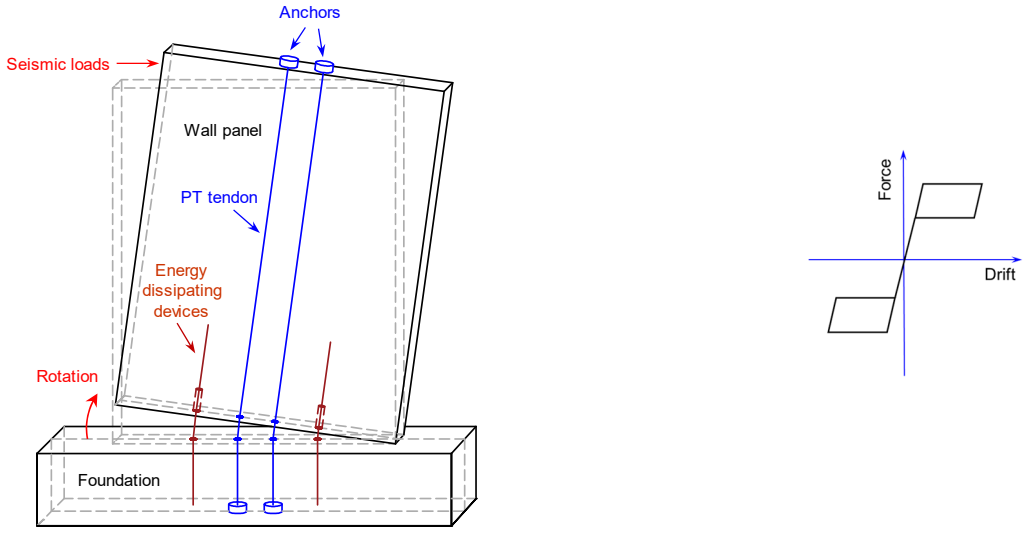

(a) Schematic configuration of the UPT wall system (b) Flag-shaped hysteretic response

Fig. 1 Schematic configuration and flag-shaped hysteretic response of the UPT wall system

determination equations of hysteretic models representing a wide range of structural systems were proposed (Priestley *et al*. 2007, Blandon and Priestley 2005). Since the hysteresis response of the UPT wall system was idealized to a flag-shaped hysteresis behavior, the EVD ratio determination of the UPT wall system can be derived from the existing EVD determination equation of bilinear hysteretic systems. In addition, researchers also have proposed different EVD ratio determination equations for the UPT wall systems (Pennucci *et al*. 2009, Priestley *et al*. 2007, Pampanin *et al*. 2010), while the influences of various EVD ratio determinations on the DDBD procedure of the UPT wall systems have not been investigated.

This study aimed to evaluate the influences of the EVD ratio determination equations for the UPT wall system with hysteretic energy dissipating devices installed at the wall base. The reinforcing bars were considered in this study as the hysteretic energy dissipating devices. The DDBD procedure with different EVD ratio determinations were carried out for the UPT wall structures with varied storey numbers. The finite element models of UPT wall systems were established in *OpenSees* (Mazzoni *et al*. 2006) to evaluate the design results. And the nonlinear time history analysis was performed for the UPT wall systems with varied storey numbers.

2. The EVD ratio determination of the UPT wall systems

The EVD ratio of a SDOF system with nonlinear hysteretic behaviour could be determined by Jacobsen's approach (Jacobsen 1930 and 1960). The EVD ratio can be obtained via equating the energy dissipated by a viscous damper with the energy dissipated from the nonlinear hysteretic behaviour of the SDOF system. The EVD ratio of a SDOF system with nonlinear hysteretic behaviour could be expressed as Eq. (1), where ξ_0 corresponding to the inherent damping, ξ_{hyst} corresponding to the EVD ratio of the hysteretic behaviour.

$$\xi_{eq} = \xi_0 + \xi_{hyst} \tag{1}$$

The hysteretic responses of the UPT wall systems were characterized as the flag-shaped response. The energy dissipating devices installed at the wall base would enhance the damping level of the UPT wall system. The λ is the ratio of the restoring moment provided by the PT tendons and energy dissipated moment provided by the energy dissipating devices. 1.25 is recommended for the λ of the UPT wall system considering material overstrength (Pampanin *et al*. 2001). The EVD ratio of the SDOF system with the flag-shaped response could be derived from the EVD ratio of the SDOF systems with the bilinear elasto-plastic hysteretic response considering energy dissipating moment contribution. The EVD ratio of the SDOF system with the flag-shaped response could be expressed in Eqs. (2) and (3) by introducing λ to the EVD ratio equation of the SDOF system with the bilinear elasto-plastic hysteresis (Rosenblueth and Herrera 1964), where μ is the ductility of the UPT wall system, r is the post yielding stiffness coefficient. And the Eq. (2) is a specific situation of the Eq. (3) with $r = 0$.

$$\xi_{eq} = \xi_0 + \xi_{hyst} = \xi_0 + \frac{2}{\pi(\lambda+1)}\frac{(\mu-1)}{\mu} \tag{2}$$

$$\xi_{eq} = \xi_0 + \xi_{hyst} = \xi_0 + \frac{2}{\pi(\lambda+1)}\frac{(\mu-1)(1-r)}{\mu(1+r\mu-r)} \tag{3}$$

Previous research has verified that the bilinear elasto-plastic hysteretic response is not conservative for the SDOF system with high ductility demand (Miranda and Ruiz-García 2002). An optimal equation of the EVD ratio of the SDOF system with the bilinear elasto-plastic hysteretic response is proposed by Blandon and Priestley (Blandon and Priestley 2005). Therefore, the EVD ratio equation of the UPT wall systems based on the optimal EVD ratio

equation of the SDOF system with the bilinear elasto-plastic hysteretic response is presented in Eq. (4). Effective period effect is considered in this optimal EVD ratio equation.

$$\xi_{eq} = \xi_0 + \xi_{hyst} = \xi_0 + \frac{f(\mu)f(T_{eff})}{(\lambda+1)N} = \xi_0 + \frac{a\left(1-\frac{1}{\mu^b}-0.1r\mu\right)\left(1+\frac{1}{(T_{eff}+c)^d}\right)\left(\frac{1}{1+(0.5+c)^d}\right)}{\pi(\lambda+1)}(\%) \quad (4)$$

In the Eq. (4), T_{eff} is the effective period and N is a normalizing factor. The calibration factors a, b, c, d for the UPT wall systems could be determined as 160, 0.5, 0.85, 4.

Researchers also have proposed modified EVD ratio equations to better define the EVD ratio for the UPT wall systems. The EVD ratio equation of the UPT wall systems could also be determined as Eq. (5) (Pampanin *et al*. 2010)

$$\xi_{eq} = \xi_0 + \xi_{hyst} = \xi_0 + \frac{R_\xi}{\lambda+1}\left(\frac{\mu-1}{\mu\pi}\right) \quad (5)$$

where R_ξ is 0.444 for RC wall/bridge.

Priestley (2003) proposed that the precast walls or frames with unbonded prestressing could be determined using Eq. (6).

$$\xi_{eq} = \xi_0 + \xi_{hyst} = \xi_0 + \frac{25}{\pi}\left(1-\frac{1}{\sqrt{\mu}}\right)(\%) \quad (6)$$

Fig. 2 compares the EVD ratio equations regarding ξ_{hyst} part of the UPT wall systems as listed above. λ = 1.25 is adopted for the EVD ratio equations. All of the predicted EVD ratios would increase with the system's ductility increasing as presented in Fig. 2. It could be seen that the EVD ratios are varied from different EVD ratio equations. The EVD ratio equation (2) predicted the largest damping level. If considering the post-yielding stiffness of the UPT wall system, the damping levels would decrease as shown in the Eq. (3). The EVD ratio calculated results of the EVD ratio Eqs. (5) and (6) are similar, and the EVD ratios were apparently reduced compared with the calculated results of the EVD ratio Eqs. (2) and (3). The EVD ratio Eq. (4) gave

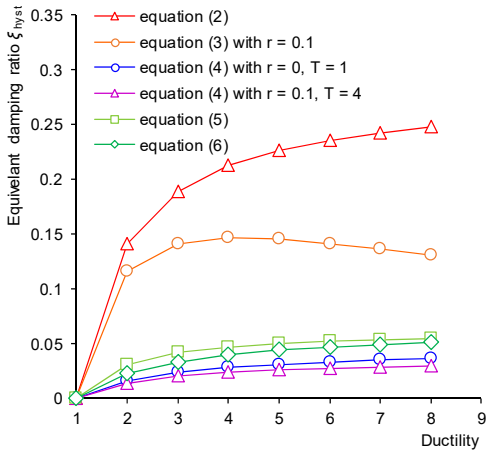

Fig. 2 Comparisons of different EVD ratio equations (ξ_{hyst} part) of the UPT wall system

the smallest EVD ratio estimation and the EVD ratio would reduce as effective period and post-yielding stiffness rise. This study investigated the influences of EVD ratio determined by the Eqs. (2), (4) and (5) on the DDBD procedure. And the EVD ratio Eqs. (2), (5) and (4) were referred to as EVD ratio determining method 1 (EVD1), 2 (EVD2) and 3 (EVD3), respectively. In this study, the inherent damping ratio of the UPT wall system was set to be 0.02 since UPT wall system was one kind of the precast concrete structural systems.

3. The DDBD procedure of the UPT wall system with different EVD ratio equations

The DDBD procedure of the UPT wall proposed by Pennucci (Pennucci *et al*. 2009) was adopted. The flow chart of the DDBD procedure is presented in Fig. 3.

Each step of the DDBD procedure for the UPT wall systems was presented below:

1. The yielding displacement profile of the UPT wall systems should be first determined in order to develop the SDOF system. Eq. (7) showed the yielding displacement at each level. The yielding displacement profile of the UPT wall systems is composed of flexural elastic deformation and wall base rotation determined by the yielding of the energy dissipating devices.

$$\Delta_{y,i} = \frac{\phi_b}{2}\left[H_i^2 - \frac{H_i^3}{2H_n} + \frac{H_i^5}{20H_n^3}\right] + \theta_{y\_base}H_i \quad (7)$$

The curvature ϕ_b at the wall base is calculated by the base moment demand. The initial value of ϕ_b is set to be 0 since the base moment demand was not known. H_i is the height of the i_{th} storey, H_n is the total height of the UPT wall system.

2. The design displacement profile of the UPT wall system is calculated by Eq. (8). A plastic rotation contribution is added to the yielding displacement profile, and this contribution could be calculated by the design limit drift θ_c and maximum drift along the wall height θ_{y_max} at yielding displacement profile. The UPT wall could be regarded as a cantilever wall, so the maximum drift is the total roof drift in the yielding displacement profile.

$$\Delta_{d,i} = \Delta_{y,i} + (\theta_c - \theta_{y\_max})H_i \quad (8)$$

3. Since the yielding and design displacement profile of the UPT wall system are determined, the MDOF system of the UPT wall could be equivalent to an equivalent SDOF system using the Eqs. (9)-(11)

$$\Delta_d = \frac{\sum_1^n m_i\Delta_{d,i}^2}{\sum_1^n m_i\Delta_{d,i}} \quad (9)$$

$$m_e = \frac{\sum_1^n m_i\Delta_{d,i}}{\Delta_d} \quad (10)$$

$$H_e = \frac{\sum_1^n m_i\Delta_{d,i}H_i}{\sum_1^n m_i\Delta_{d,i}} \quad (11)$$

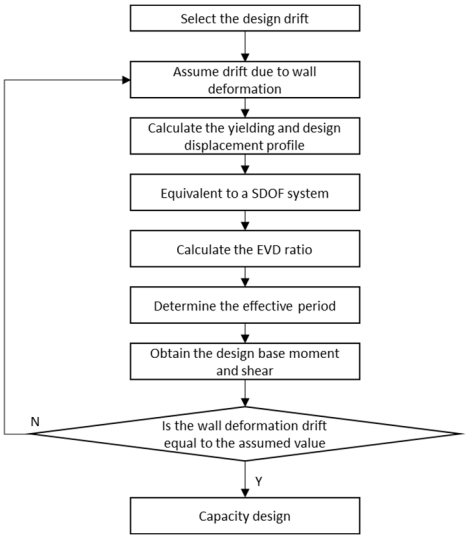

Fig. 3 Flow chart of the DDBD procedure for the UPT wall systems

where m_i is the seismic mass of the i_{th} storey, Δ_d, m_e and H_e are the design displacement, effective mass and effective height of the equivalent SDOF system.

And the ductility demand of the equivalent SDOF system could be determined by Eq. (12).

$$\mu = \frac{\Delta_d}{\Delta_{y,H_e}} \tag{12}$$

4. The EVD ratio could be determined by the selected equations as discussed in Section 2.

5. The EVD ratio of the equivalent SDOF system could be adopted to obtain a damping-dependent scaling factor η as presented in Eq. (13) (European Standard EN 2005). A lower boundary value is set for η and the η should not exceed 1. The reduced design displacement spectrum is calculated by Eq. (14). The effective period T_{eff} of the equivalent SDOF system could be determined by the reduced design displacement spectrum and the design displacement Δ_d value.

$$\eta = \sqrt{\frac{0.07}{0.02+\xi}} \geq 0.55 \tag{13}$$

$$\Delta(T,\xi) = \eta \cdot \Delta(T, 5\%) \tag{14}$$

6. The base shear at design displacement is determined by Eq. (15).

$$F_d = \left(\frac{2\pi}{T_{eff}}\right)^2 m_e \Delta_d \tag{15}$$

7. If the wall deformation drift is convergence, section design of the UPT wall systems should be performed.

4. Case study structures and the DDBD procedure results

The case study structures are four-storey (4DOF), twelve-storey (12DOF), twenty-storey (20DOF) precast concrete wall structures. The typical plan and elevation layouts of the case study building with twelve-storey are shown in Fig. 4. The UPT wall systems were arranged along the longitudinal direction as lateral resisting systems. The frames in the longitudinal direction were gravity frames carrying vertical loads. The gravity load and geometric information for the case study structures are presented in Table 1. Each storey height and weight are the same for the case study structures with varied storey numbers. The design limit drift under design earthquake level is 2%, the design earthquake level is corresponding to the rare earthquake intensity. The ratio λ of the restoring moment and the energy dissipated moment is 1.25. In this study, the design spectrum is based on the Chinese Code (PRC National Standard 2010b) considering rare earthquake intensity, the maximum horizontal earthquake influence coefficient α_{max} of 1.2 is adopted. The seismic site design is Group 2 and Site Class II, with characteristic period T_g

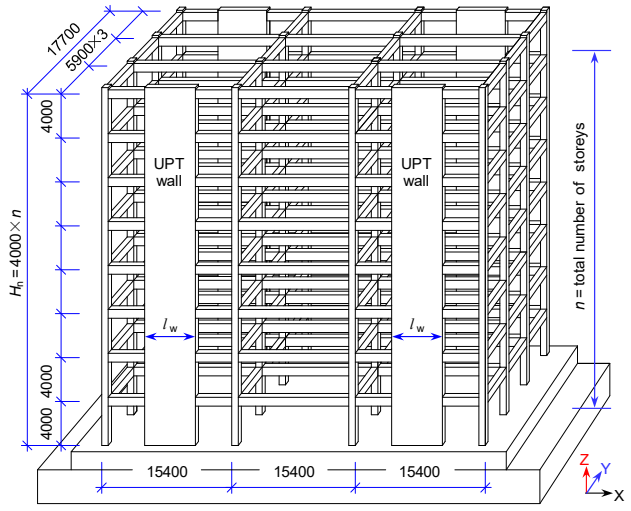

Fig. 4 Plan and elevation layouts of a twelve-storey case study structurey

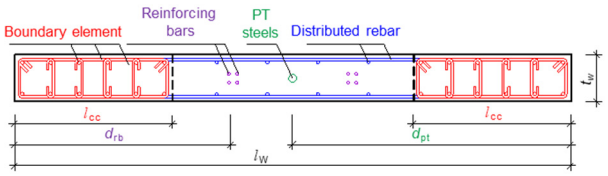

(a) 4DOF case study structure

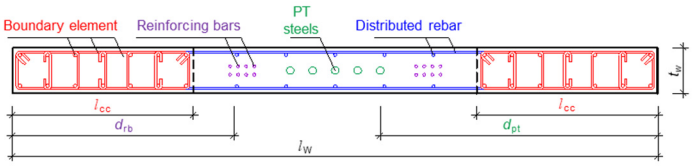

(b) 12DOF case study structure

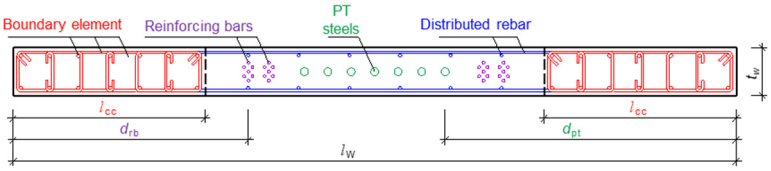

(c) 20DOF case study structurey

Fig. 5 Cross sections layouts of the UPT wall bases

Table 1 Geometry and gravity load of case study structures

n	4	12	20
Wall length (mm)	4000	7000	9000
Wall thickness (mm)	320	380	500
Inter-storey height (m)	4000	4000	4000
Wall axial load ratio* (%)	3.55	6.01	6.34
Mass at each level per wall (ton)	125	125	125

*The wall axial load ratio calculation was corresponded to EVD1

equaling to 0.4 s.

The arrangements of reinforcing bars and PT steels at UPT wall base cross sections are shown in Fig. 5, the PT steels were arranged at the centerline of the wall section, and the reinforcing bars were incorporated at the outside of the PT steels. The d_{pt} is the distance between the outmost PT steel to the nearest wall edge. The d_{rb} is the distance between the centroid of the outmost reinforcing bar group to the nearest wall edge. The interval between PT steels and the interval between centroids of reinforcing bars are both 200 mm. l_{cc} is the length of the confined concrete region, which is always larger than the neutral axis depth c.

The design results of each case study structures are summarized in Table 2. For different storeys of the case study structures, three types of EVD ratio equations were adopted in the DDBD procedure, respectively. Therefore, there are total nine design results considering different storeys and different EVD ratio equations. Each design result is named as "number of DOF – EVD ratio determining method". Table 2 shows that the ductility of the UPT wall systems decreased with the number of the structures total storey increasing since the flexural deformation of the wall panels increased. The strength demand of structures with EVD1 is the smallest compared with those of the structures with EVD2 and EVD3. The design strength of the UPT wall was always the smallest by adopting EVD1 and the largest by adopting EVD3.

Based on the design results of the DDBD procedure, the

Table 2 DDBD results of case study structures

	Δ_y (mm)	Δ_d (mm)	μ	ξ_{eq} (%)	T_{eff} (s)	Base shear (kN)	Base moment (kN·m)
4DOF-EVD1	11.9	237	19.77	28.88	2.54	2407	28940
4DOF-EVD2	14.2	236.1	16.62	9.52	2.09	3546	42655
4DOF-EVD3	17	235	13.85	5.9	1.8	4737	57028
12DOF-EVD1	64.9	642	9.89	27.45	4.64	5445	182651
12DOF-EVD2	79.6	634.5	7.97	8.99	3.63	8734	293586
12DOF-EVD3	81.7	633	7.76	5.37	3.2	11105	373400
20DOF-EVD1	119.7	1048.1	8.75	27.07	6	8706	479326
20DOF-EVD2	148.4	1031.3	6.95	8.85	4.95	12516	691049
20DOF-EVD3	190.7	1011.5	5.3	5	4.22	16742	927667

Table 3 Section design of the UPT wall bases

	4DOF			12DOF			20DOF		
	EVD1	EVD2	EVD3	EVD1	EVD2	EVD3	EVD1	EVD2	EVD3
Concrete compressive strength f_c'(MPa)	35	45	50	40	60	80	80	88	90
Confined concrete compressive strength f_{cc}' (MPa)	45.9	63	77	48	93.6	144	104.8	176	198
l_{cc}/l_w		0.25			0.286			0.311	
c/l_w	0.11	0.13	0.15	0.18	0.14	0.11	0.23	0.16	0.17
f_{pti}/f_{ptk}	0.41	0.53	0.58	0.44	0.42	0.5	0.35	0.46	0.62
d_{pt} (mm)		2000			3100			3900	
n_{pt}	3	6	9	2	7	9	3	7	10
$l_{un,rb}$ (mm)		400			600			800	
Φ_{rb} (mm)	25	30	36	37	44	49	40	44	54
d_{rb} (mm)		1500			2700			3500	

wall base section designs are presented in Table 3. The material properties of PT steels and reinforcing bars were corresponding to the Chinese Code (PRC National Standard 2010a). 1×7 ϕ17.8 strand was used as PT steels in the UPT wall with 1860 MPa tensile yielding stress f_{ptk}. The ratio of the PT steels initial stress and the tensile yielding stress was f_{pti}/f_{ptk}. The number of strands in each PT steel location was represented by n_{pt}. The yielding stress of reinforcing bars was 400 MPa. The unbounded length $l_{un,rb}$ and diameter Φ_{rb} of the reinforcing bars were also listed in Table 3. It should be noticed that the concrete strength determined by the EVD3 was large, and the values of the concrete strength were only for design and analysis purposes.

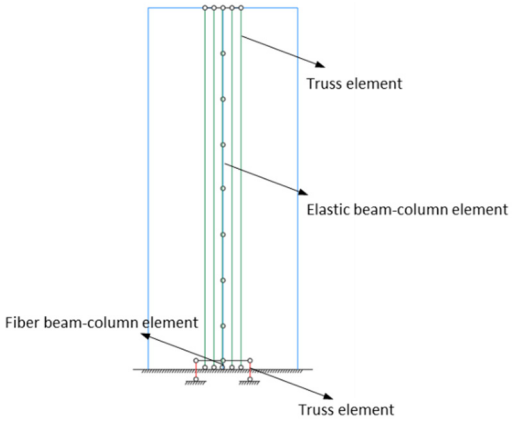

Fig. 6 Schematic layout of the UPT wall model

5. Evaluation of the EVD ratio determination influence on the DDBD procedure

In this study, numerical finite element models were established to validate the design results. Since the UPT wall systems were arranged along longitudinal direction as lateral resisting systems and the gravity frames along longitudinal direction were designed to carry the vertical loads, a single UPT wall model was adopted for nonlinear time history analysis. The single UPT wall was modelled by the fiber hinge element model. The fiber hinge element model was validated with system-level test building results (Gu *et al*. 2022). The schematic layout of the UPT wall finite element models is shown in Fig. 6. A nonlinear fiber beam-column element was used to represent the nonlinear rocking mechanism at the wall base, and the critical height H_{cr} in this study was set to be t_w. The concrete02 material was adopted for unconfined and confined concrete fibers. PT steels and reinforcing bars were modelled by truss elements with Steel02 materials. The fundamental periods of the models were dominated by the total storey numbers while not sensitive to the variant of the concrete strength, diameters of the reinforcing bars and initial force of the PT steels in the wall base section. The fundamental periods of the models designed with EVD3 were 0.55 sec, 1.68 sec and 2.39 sec corresponding to the 4DOF, 12DOF and 20DOF structures. The fundamental periods of the models with EVD1 and EVD2 were similar to those of the models with EVD3 under the same total storey numbers.

5 ground motions from PEER database (Ancheta *et al*. 2014) and 2 artificial waves were selected as the ground motion set. The information of the selected ground motion is listed in Table 4. According to the Chinese Code (PRC National Standard 2010b), the PGAs of the seismic records were all scaled to 510 cm/s. Fig. 7 shows the spectral responses of the ground motion set and the design spectrum, and the average spectrum of the ground motion set are matched with the design spectrum.

The global responses of the case study structures were investigated. Fig. 8 presents the average peak inter-storey drifts of each case study structure. The peak inter-storey

Table 4 GM information

Ground motion	Year	Station	Magnitude
San Fernando	1971	Maricopa Array #2	6.61
Hector Mine	1999	Snow Creek	7.13
Chi-Chi, Taiwan-04	1999	CHY114	6.2
Chi-Chi, Taiwan-04	1999	HWA051	6.2
Niigata, Japan	2004	CHB014	6.63

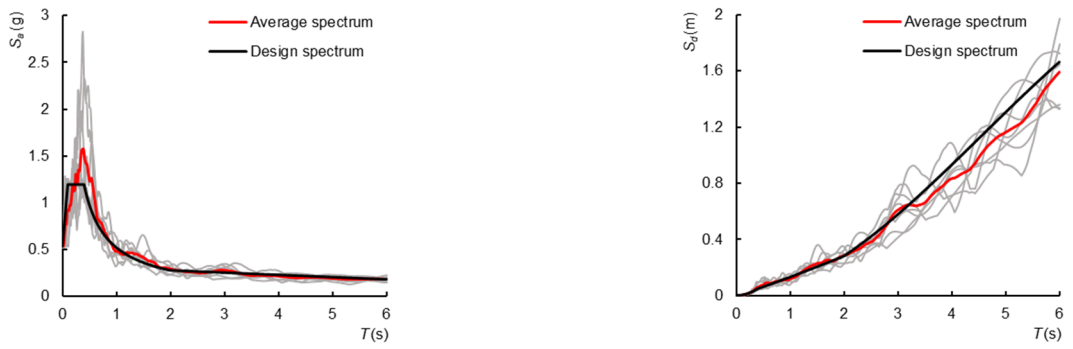

(a) Acceleration spectra (b) Displacement spectra

Fig. 7 Spectral responses of the ground motion set and design spectrum

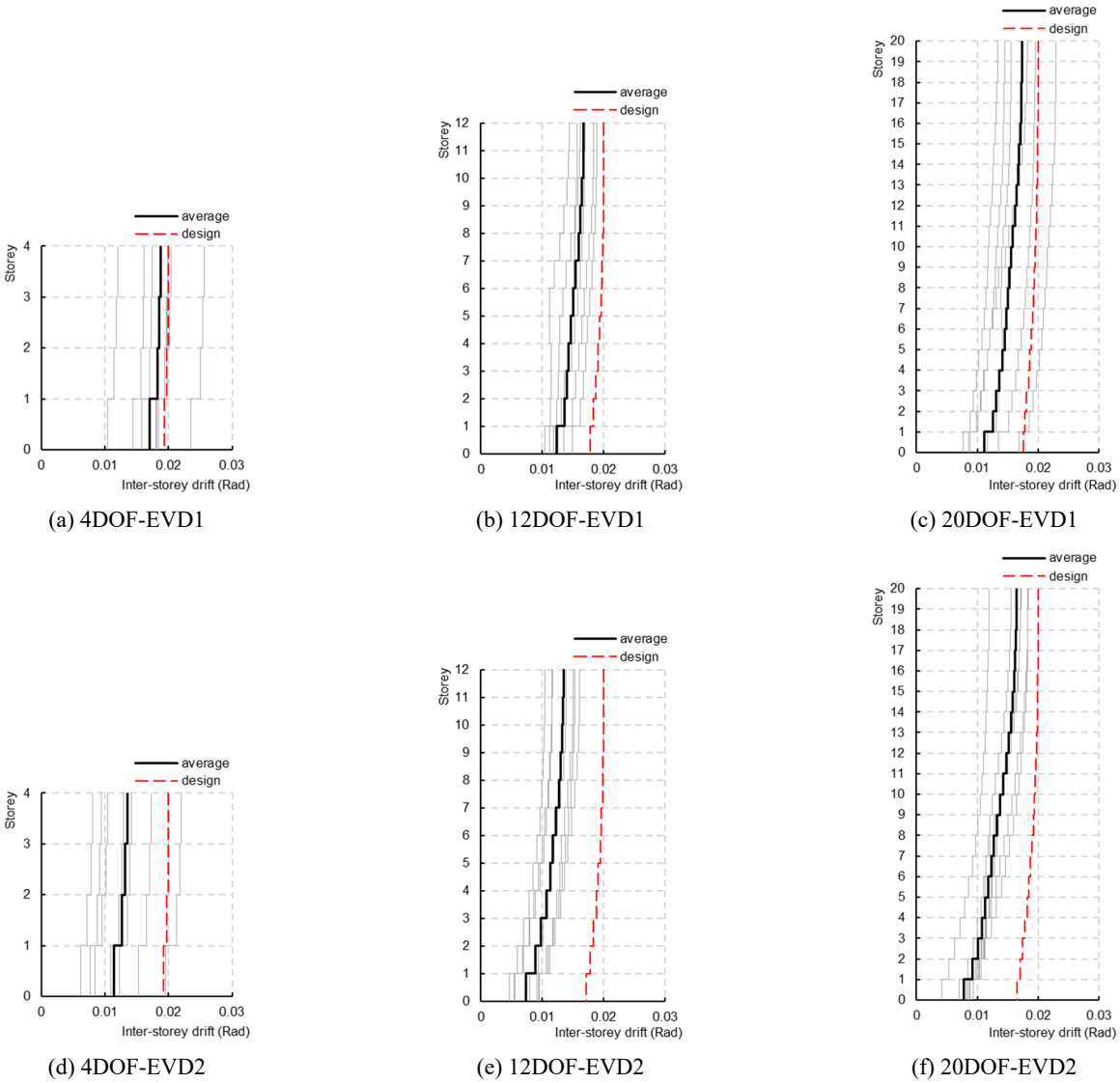

(a) 4DOF-EVD1 (b) 12DOF-EVD1 (c) 20DOF-EVD1

(d) 4DOF-EVD2 (e) 12DOF-EVD2 (f) 20DOF-EVD2

Fig. 8 Peak inter-storey drifts for case study structures

drifts under each seismic record were represented by grey solid lines in subplots. Since the DDBD procedure aimed to control the storey drift, the average peak inter-storey drift could be selected to verify the design procedure. The average peak inter-storey drifts of all the case study structures were all below the design limit drift, and the inter-storey drift at roof level was closest to the design limit drift. The peak inter-storey drift results of case study structures with EVD1 best matched with the design inter-storey drifts considering three different total storey

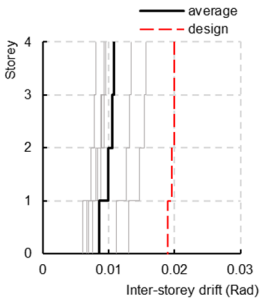

(g) 4DOF-EVD3

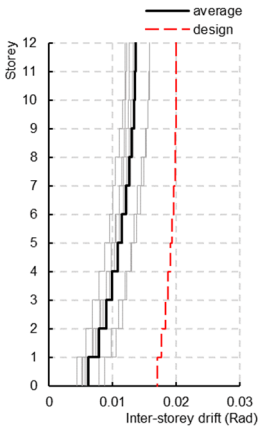

(h) 12DOF-EVD3

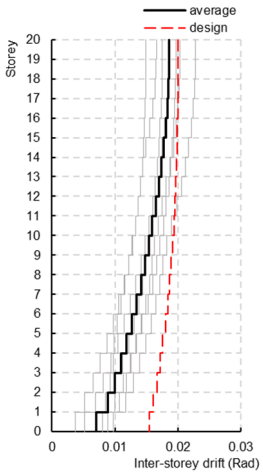

(i) 20DOF-EVD3

Fig. 8 Continued

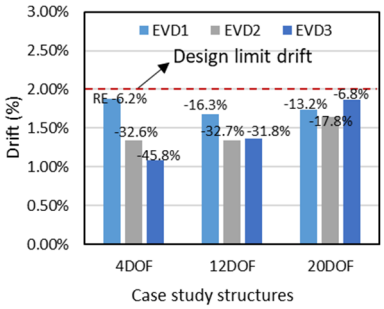

Fig. 9 Peak inter-storey drifts and REs at roof level for case study structures

numbers. The difference between peak inter-storey drifts of the nonlinear time histories and the design inter-storey drifts were more significant for the case study structures with EVD2 and EVD3. The peak inter-storey drift at roof level and the corresponding relative errors (REs) regarding the design limit drift of each case study structure are presented in Fig. 9. The REs of peak inter-storey drift at roof level would decrease as the storeys of the structures considering EVD2 and EVD3 rises. Comparison of the REs of the inter-storey drift at roof level for case study structures showed that the case study structures with EVD1 predicted the inter-storey drift aligned to the design limit drift at roof level considering all the total storey numbers.

Fig. 10 presents the peak moments along the wall height of each case study structure. The average peak base moments of all the case study structures were comparable to the designed base moments. This observation indicated the established numerical model was correct for the DDBD results. However, higher mode effects were found for twelve-storey and twenty-storey case study buildings. The moment profiles of twelve-storey and twenty-storey case study structures have displayed that the moment responses at upper storeys were larger than the design values. The maximum difference between the simulated moment and the design moment occurred at the mid-height of the

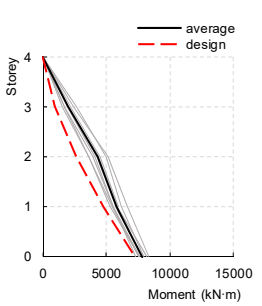

(a) 4DOF-EVD1

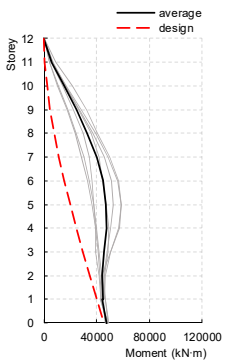

(b) 12DOF-EVD1

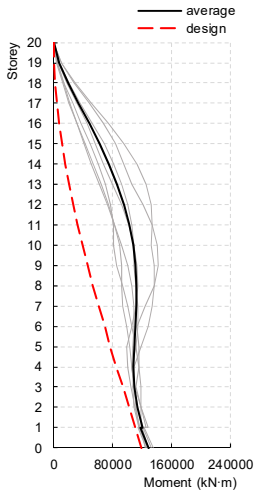

(c) 20DOF-EVD1

Fig. 10 Peak moment profiles for case study structures

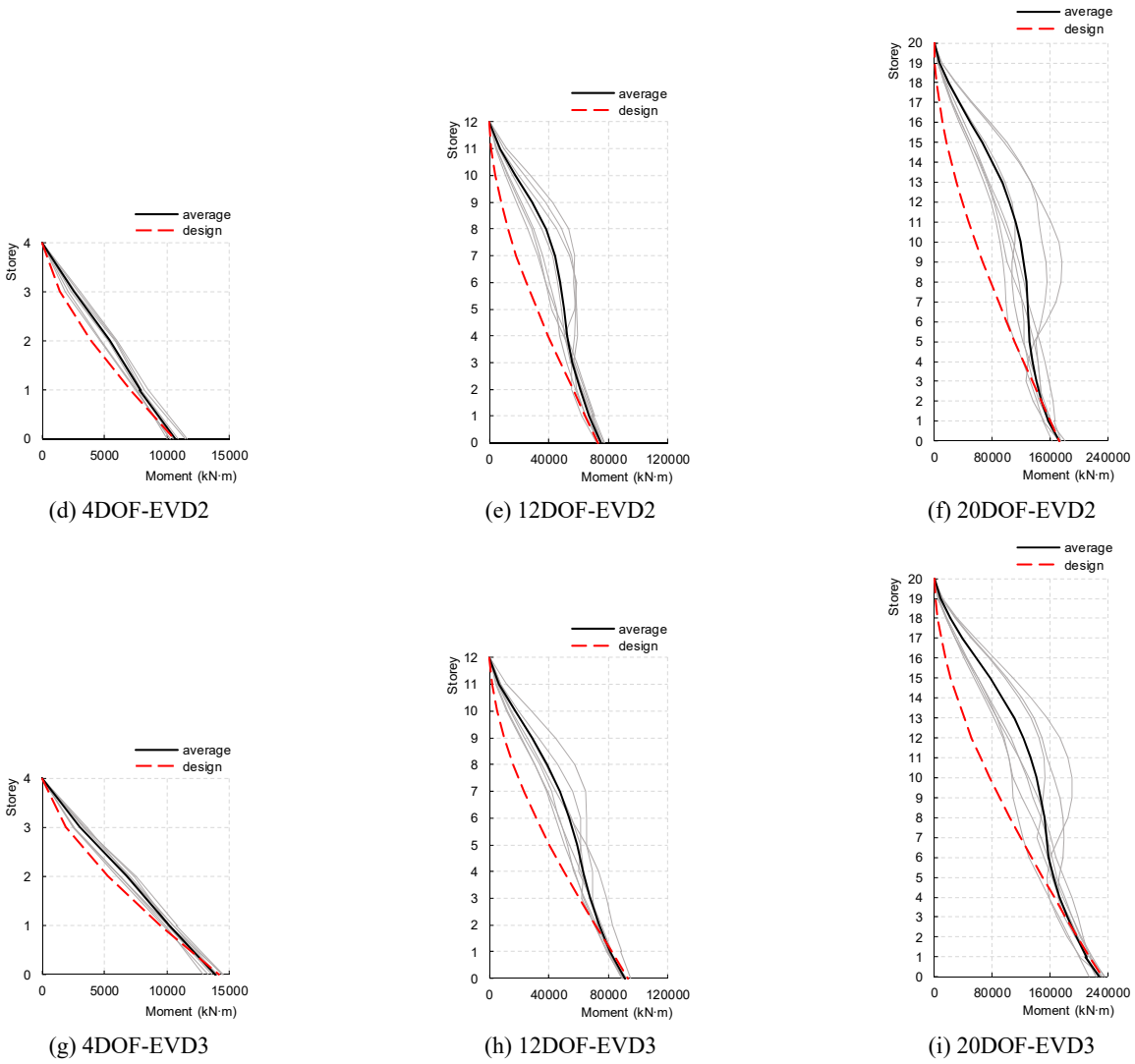

(d) 4DOF-EVD2 (e) 12DOF-EVD2 (f) 20DOF-EVD2

(g) 4DOF-EVD3 (h) 12DOF-EVD3 (i) 20DOF-EVD3

Fig. 10 Continued

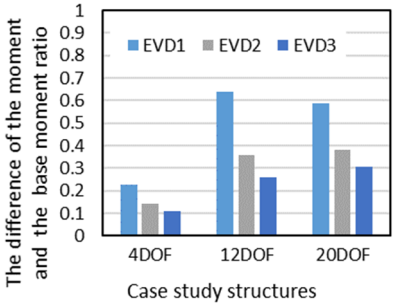

Fig. 11 The maximum moment amplification in each case study structure

structures. Fig. 11 illustrates the ratio of the maximum difference between the simulated moment and the design moment and the base moment in each case study structure. And the moment magnification was most significant for case study structures designed with EVD1. The moment responses have indicated the capacity design of upper wall panels should consider higher mode effect. Wiebe and Christopoulos (2009) have discussed the mitigation of the higher mode effect by using multiple rocking sections of UPT walls.

6. Conclusions

In this study, the influences of the EVD ratio determination on the DDBD procedure of the UPT wall systems were investigated. The DDBD procedures with three different EVD ratio determinations were carried out for UPT wall systems with different total storey numbers. The planar models of UPT walls were established in *OpenSees* to evaluate the design results of the DDBD procedures. And the nonlinear time history analysis was performed to obtain the dynamic responses of the case study structures with varied total storey numbers. The conclusions drawn from the analysis were listed below:

(1) From the design results of DDBD procedures considering different EVD ratio determinations, the strength demand of the design procedure would increase with more conservative EVD ratio estimation.

(2) From the nonlinear time history analysis, the average inter-storey drifts of all the case study structures were all below the design limit drift. Comparison of the peak inter-storey drift of the case study structures designed by different EVD ratio determinations showed the peak inter-storey drifts of the case study structures with EVD1 best matched to the design limit drift.

(3) From the nonlinear time history analysis, the average peak base moments of all the case study structures were comparable to the designed base moments. Nevertheless, higher mode effects were found for twelve-storey and twenty-storey case study structures. The moment responses have indicated the capacity design of upper wall panels should consider higher mode effect.

(4) The design results of the DDBD procedure with three different EVD ratio determinations for four-storey UPT wall systems were all acceptable. However, the structures designed with EVD1 would have significant moment magnification as the total storey numbers increased. The EVD1 predicted the highest damping ratio, so the design displacement of the equivalent SDOF system of twenty-storey structures would exceed the design displacement spectra. The EVD3 predicted the lowest damping ratio, which would be smaller than 5% in twenty-storey UPT wall systems, so the strength demand of the UPT wall systems with the EVD3 was difficult to achieve. Hence, the EVD2 was more suitable for the twelve-storey and twenty-storey UPT wall systems based on the intensity, site and the ground motion set selected in this study. More case studies considering different intensities, sites and ground motion sets should be performed to further investigate the appropriate EVD ratio determination of the DDBD procedure considering the UPT wall systems.

Acknowledgments

The authors are grateful for financial support from Japan Society for the Promotion of Science (Grant No. P22371), and the financial support provided by a Rutherford Discovery Fellowship.

References

Ancheta, T.D., Darragh, R.B., Stewart, J.P., Seyhan, E., Silva, W.J., Chiou, B.S.J., Wooddell, K.E., Graves, R.W., Kottke, A.R., Boore, D.M. and Kishida, T. (2014), "NGA-West2 database", *Earthq. Spectra*, **30**(3), 989-1005. https://doi.org/10.1193/070913EQS197M

Bedriñana, L.A., Tani, M. and Nishiyama, M. (2021), "Deformation and cyclic buckling capacity of external replaceable hysteretic dampers for unbonded post-tensioned precast concrete walls", *Eng. Struct.*, **235**, p. 112045. https://doi.org/10.1016/j.engstruct.2021.112045

Blandon, C.A. and Priestley, M.J.N. (2005), "Equivalent viscous damping equations for direct displacement based design", *J. Earthq. Eng.*, **9**(sup2), 257-278. https://doi.org/10.1142/S1363246905002390

Erkmen, B. and Schultz, A.E. (2009), "Self-centering behavior of unbonded, post-tensioned precast concrete shear walls", *J. Earthq. Eng.*, **13**(7), 1047-1064. https://doi.org/10.1080/13632460902859136

European Standard EN (Eurocode 8 1998-1). (2005), Design of structures for earthquake resistance-part 1: general rules, seismic actions and rules for buildings, Bruxelles, European Committee for Standardization (CEN).

Gu, A., Zhou, Y., Xiao, Y., Li, Q. and Qu, G. (2019), "Experimental study and parameter analysis on the seismic performance of self-centering hybrid reinforced concrete shear walls", *Soil Dyn. Earthq. Eng.*, **116**, 409-420. https://doi.org/10.1016/j.soildyn.2018.10.003

Gu, A., Zhou, Y., Henry, R.S., Lu, Y. and Rodgers, G.W. (2022), "Simulation of shake-table test for a two-story low-damage concrete wall building", *Struct. Control Health Monitor.*, **29**(10), p. e3038. https://doi.org/10.1002/stc.3038

Holden, T., Restrepo, J. and Mander, J.B. (2003), "Seismic performance of precast reinforced and prestressed concrete walls", *J. Struct. Eng.*, **129**(3), 286-296. https://doi.org/10.1061/(ASCE)0733-9445(2003)129:3(286)

Huang, H.B., Yi, T.H., Li, H.N. and Liu, H. (2020), "Strain-based performance warning method for bridge main girders under variable operating conditions", *J. Bridge Eng.*, **25**(4), 04020013. https://doi.org/10.1061/(ASCE)BE.1943-5592.0001538

Jacobsen, L.S. (1930), "Steady forced vibration as influenced by damping", *Transact. ASME*, **52**(15), 169-181.

Jacobsen, L.S. (1960), "Damping in composite structures", *Proceedings of the 2nd World Conference on Earthquake Engineering*, Tokyo, Japan.

Kurama, Y., Pessiki, S., Sause, R. and Lu, L.W. (1999), "Seismic behavior and design of unbonded post-tensioned precast concrete walls", *PCI J.*, **44**(3), 72-89. https://doi.org/10.15554/pcij.05011999.72.89

Liu, R., McHaffie, B. and Palermo, A. (2018), "Improving post-tensioned rocking bridge columns for large and multiple earthquake events", *The 17th US-Japan-New Zealand Workshop on the Improvement of Structural Engineering and Resilience*, Queenstown, New Zealand.

Mazzoni, S., McKenna, F., Scott, M.H. and Fenves, G.L. (2006), "OpenSees command language manual", *Pacific Earthquake Engineering Research (PEER) Center*, **264**(1), 137-158.

Mander, J.B., Priestley, M.J. and Park, R. (1988), "Theoretical stress-strain model for confined concrete", *J. Struct. Eng.*, **114**(8), 1804-1826.

Miranda, E. and Ruiz-García, J. (2002), "Evaluation of the approximate methods to estimate maximum inelastic displacement demands", *Earthq. Eng. Struct. Dyn.*, **31**(3), 539-560. https://doi.org/10.1002/eqe.143

Nagae, T., Matsumori, T., Shiohara, H., Kabeyasawa, T., Kono, S., Nishiyama, M., Moehle, J., Wallace, J., Sause, R. and Ghannoum, W. (2014), "The 2010 E-defense shaking table test on four-story reinforced concrete and post-tensioned concrete buildings", *Proceedings of the 10th US National Conference on Earthquake Engineering (NCEE), Frontiers of Earthquake Engineering*, Anchorage, Alaska, USA.

Pampanin, S., Priestley, M.N. and Sritharan, S. (2001), "Analytical modelling of the seismic behaviour of precast concrete frames designed with ductile connections", *J. Earthq. Eng.*, **5**(3), 329-367.

Pampanin, S., Marriott, D. and Palermo, A. (2010), "PRESSS design handbook", Auckland, New Zealand, New Zealand Concrete Society.

Pennucci, D., Calvi, G.M. and Sullivan, T.J. (2009), "Displacement-based design of precast walls with additional dampers", *J. Earthq. Eng.*, **13**(S1), 40-65. https://doi.org/10.1080/13632460902813265

Perez, F.J., Sause, R. and Pessiki, S. (2007), "Analytical and experimental lateral load behavior of unbonded posttensioned precast concrete walls", *J. Struct. Eng.*, **133**(11), 1531-1540.

https://doi.org/10.1061/(ASCE)0733-9445(2007)133:11(1531)
PRC National Standard (GB 50010-2010) (2010a), Code for design of concrete structures, China Architecture & Building Press, Beijing, China. [In Chinese]
PRC National Standard (GB 50011-2010) (2010b), Code for seismic design of buildings, China Architecture & Building Press, Beijing, China. [In Chinese]
Priestley, M.N. (2002), "Direct displacement-based design of precast/prestressed concrete buildings", *PCI J.*, **47**(6), 66-79. https://doi.org/10.15554/pcij.11012002.66.79
Priestley, M.N. (2003), "Myths and fallacies in earthquake engineering, revisited: The ninth mallet Milne lecture", Pavia, Italy, IUSS press.
Priestley, M.J.N., Calvi, G.M. and Kowalsky, M.J. (2007), "Direct displacement-based seismic design of structures", In: *New Zealand Conference on Earthquake Engineering*, Auckland, New Zealand.
Rahman, M.A. and Sritharan, S. (2006), "An evaluation of force-based design vs. direct displacement-based design of jointed precast post-tensioned wall systems", *Earthq. Eng. Eng. Vib.*, **5**(2), 285-296. https://doi.org/10.1007/s11803-006-0620-3
Restrepo, J.I. and Rahman, A. (2007), "Seismic performance of self-centering structural walls incorporating energy dissipators", *J. Struct. Eng.*, **133**(11), 1560-1570.
Rosenblueth, E. and Herrera, I. (1964), "On a kind of hysteretic damping", *J. Eng. Mech. Div.*, **90**(4), 37-48.
Smith, B.J., Kurama, Y.C. and McGinnis, M.J. (2011), "Design and measured behavior of a hybrid precast concrete wall specimen for seismic regions", *J. Struct. Eng*, **137**(10), 1052-1062. https://doi.org/10.1061/(ASCE)ST.1943-541X.0000327
Van der Meer, L.J., Martens, D.R.W. and Vermeltfoort, A.T. (2013), "UPT rectangular and flanged shear walls of high-strength CASIEL-TLM masonry: Experimental and numerical push-over analysis", *Eng. Struct.*, **49**, 628-642. https://doi.org/10.1016/j.engstruct.2012.11.021
Watkins, J., Sritharan, S., Nagae, T. and Henry, R.S. (2017), "Computational modelling of a four storey post-tensioned concrete building subjected to shake table testing", *Bull. New Zealand Soc. Earthq. Eng.*, **50**(4), 595-607. https://doi.org/10.5459/bnzsee.50.4.595-607
Wiebe, L. and Christopoulos, C. (2009), "Mitigation of higher mode effects in base-rocking systems by using multiple rocking sections", *J. Earthq. Eng.*, **13**(S1), 83-108. https://doi.org/10.1080/13632460902813315
Zheng, X., Yi, T.H., Yang, D.H. and Li, H.N. (2021), "Stiffness estimation of girder bridges using influence lines identified from vehicle-induced structural responses", *J. Eng. Mech.*, **147**(8), 04021042. https://doi.org/10.1061/(ASCE)EM.1943-7889.0001942